Polarized human cholangiocytes release distinct populations of apical and basolateral small extracellular vesicles

Brian A. Davies[a], Leslie O. Morton[b,†], John R. Jefferson[b,c], Cody N. Rozeveld[a,d], Luke C. Doskey[a,d], Nicholas F. LaRusso[a,b], and David J. Katzmann[a,d,*]

[a]Biochemistry and Molecular Biology Department; [b]Division of Gastroenterology and Hepatology, and [d]Mayo Clinic Graduate School of Biomedical Science, Mayo Clinic, Rochester, MN 55905; [c]Chemistry Department, Luther College, Decorah, IA 52101

ABSTRACT **Intercellular communication is critical for organismal homeostasis, and defects can contribute to human disease states. Polarized epithelial cells execute distinct signaling agendas via apical and basolateral surfaces to communicate with different cell types. Small extracellular vesicles (sEVs), including exosomes and small microvesicles, represent an understudied form of intercellular communication in polarized cells. Human cholangiocytes, epithelial cells lining bile ducts, were cultured as polarized epithelia in a Transwell system as a model with which to study polarized sEV communication. Characterization of isolated apically and basolaterally released EVs revealed enrichment in sEVs. However, differences in apical and basolateral sEV composition and numbers were observed. Genetic or pharmacological perturbation of cellular machinery involved in the biogenesis of intralumenal vesicles at endosomes (the source of exosomes) revealed general and domain-specific effects on sEV biogenesis/release. Additionally, analyses of signaling revealed distinct profiles of activation depending on sEV population, target cell, and the function of the endosomal sorting complex required for transport (ESCRT)-associated factor ALG-2–interacting protein X (ALIX) within the donor cells. These results support the conclusion that polarized cholangiocytes release distinct sEV pools to mediate communication via their apical and basolateral domains and suggest that defective ESCRT function may contribute to disease states through altered sEV signaling.**

Monitoring Editor
Jennifer Lippincott-Schwartz
Howard Hughes Medical Institute

Received: Mar 4, 2019
Revised: Aug 7, 2020
Accepted: Aug 19, 2020

INTRODUCTION

Canonical intercellular communication involves the release of small soluble molecules from donor cells that bind to receptors on the surface or within the cytosol of target cells to elicit effects. Additionally, extracellular vesicles (EVs) released from donor cells can influence target cells both through ligands present on the surface of the particles and via factors contained within the lumen of the vesicles, including signaling molecules and microRNAs (miRNAs) (Colombo *et al.*, 2014; Hirsova *et al.*, 2016b; Maas *et al.*, 2017). Intercellular communication is further complicated by the existence of polarized epithelia wherein domain-specific signaling may occur via the distinct apical and basolateral domains, and domain-specific EV release from polarized epithelia or organoids have been reported (van Niel *et al.*, 2001; Tauro *et al.*, 2013; Ji *et al.*, 2014; Chen *et al.*, 2016; Klingeborn *et al.*, 2017; Chin *et al.*, 2018).

Three general classes of EVs have been described: apoptotic bodies, microvesicles, and exosomes (Mathieu *et al.*, 2019). These EVs differ in their sizes, contents, and mechanisms of biogenesis. Apoptotic bodies (>500 nm) are generated by large-scale membrane blebbing, whereas microvesicles (50–1000 nm) bud from the plasma membrane. Small microvesicles are similar in size and density to another EV class, exosomes, although their biogenesis is distinct. Exosomes are derived from an intracellular sorting process

This article was published online ahead of print in MBoC in Press (http://www.molbiolcell.org/cgi/doi/10.1091/mbc.E19-03-0133) on August 26, 2020.

Conflicts of interest: The authors declare they have no conflicts of interest with the contents of this article.

†Present address: Pfizer Oncology, New York, NY 27599.

*Address correspondence to: David J. Katzmann (katzmann.david@mayo.edu).

Abbreviations used: ALIX, ALG-2–interacting protein X; ESCRT, endosomal sorting complex required for transport; EV, extracellular vesicle; ILV, intralumenal vesicle; MVE, multivesicular endosome; NHC, normal human cholangiocyte; N-SMase, neutral-sphingomylinase; sEV, small extracellular vesicle.

wherein the limiting membrane of endosomes buds inward to generate 50–150 nm intralumenal vesicles (ILVs) within multivesicular endosomes (MVEs). While MVEs are most commonly associated with lysosomal degradation of transmembrane proteins delivered to the endosomal network, heterotypic fusion of a MVE with the plasma membrane releases these ILVs as exosomes. Exosome biogenesis has been a topic of intense investigation, revealing roles for a variety of proteins and lipid species (Hessvik and Llorente, 2018; Skotland *et al.*, 2019). Endosomal sorting complex required for transport (ESCRT) factors represent conserved machinery mediating MVE sorting from yeast to mammals (Christ *et al.*, 2017; Schoneberg *et al.*, 2017), and the ESCRT-associated factor ALG-2–interacting protein X (ALIX) has been implicated in exosome biogenesis both generally (Larios *et al.*, 2020) and by linking the Syndecan-syntenin function during cargo selection with the ESCRT-III membrane remodeling machinery responsible for ILV generation (Baietti *et al.*, 2012). Additionally, an alternate and potentially ESCRT-independent pathway of MVE formation involving ceramide generation by neutral-sphingomylinase (N-SMase) has also been implicated in exosome biogenesis (Trajkovic *et al.*, 2008). The contributions of ESCRT-dependent and -independent pathways to polarized EV biogenesis and release in epithelia have not been addressed. In addition to facilitating ILV formation on endosomes, the ESCRT machinery has been observed associated with the plasma membrane (Hanson *et al.*, 2008) and ESCRT function has been implicated in release of small microvesicles in addition to exosome biogenesis (Jackson *et al.*, 2017). These small microvesicles and exosomes may copurify during standard exosome isolation procedures, and we will thus refer to the vesicles we are studying as small extracellular vesicles (sEVs) by current convention (Thery *et al.*, 2018).

The liver consists of a variety of cell types (e.g., hepatocytes, stellate cells, cholangiocytes), and intercellular communication is critical to maintain normal organ function. Cholangiocytes, the epithelial cells that line the biliary tree, contribute to the generation of bile and participate in liver repair and in some contexts to liver injury (O'Hara *et al.*, 2013; Cheung *et al.*, 2018). Dysfunction of the cholangiocyte is associated with a range of diseases called cholangiopathies, including a number of inflammatory, genetic, malignant, and infectious diseases (Lazaridis and LaRusso, 2016; Banales *et al.*, 2019). Many of the cholangiopathies are characterized by significant morbidity and mortality and, for some, liver transplantation is the primary therapeutic intervention (Eaton *et al.*, 2013; Hirschfield *et al.*, 2013). Abnormal intercellular signaling has emerged as a candidate in these disease processes. An increase in the levels of biliary sEVs has been observed in a cholangiopathy animal model (Masyuk *et al.*, 2010), and cholangiocytes derived from patients with primary sclerosing cholangitis (PSC) exhibit increased EV release (Al Suraih *et al.*, 2020). In addition, EV-associated biomarkers have been identified as potential indicators of disease onset and/or progression (Arbelaiz *et al.*, 2017; Julich-Haertel *et al.*, 2017; Olaizola *et al.*, 2018). As cholangiocytes are polarized epithelial cells, these observations have led us to test the hypothesis that cholangiocytes mediate distinct sEV-based communication with different target cells via their apical and basolateral domains to support liver homeostasis.

An in vitro system culturing normal human cholangiocytes (NHC) as polarized epithelia in Transwells allowing collection of cultured media from apical and basolateral fractions was developed and validated. EVs derived from this system exhibited characteristics consistent with sEV enrichment, and, as hypothesized, differences were observed between the apical and basolateral sEV populations, most relevantly in the context of target cell signaling. In addition, depletion of ALIX altered polarized sEV release and communication, suggesting that this ESCRT-associated factor contributes to polarized release in a domain-specific manner. These results are consistent with the model that cholangiocytes release distinct populations of sEVs from their apical and basolateral surfaces to mediate domain-specific intercellular communication and establish a model with which to further investigate this phenomenon.

RESULTS

NHCs form a restrictive epithelial layer in a Transwell culture model

The biliary epithelial model used in these studies is the NHC cell line derived from nondiseased patient tissue (Joplin *et al.*, 1989). Transwell culturing resulted in the formation of a restrictive layer of NHC cells that is stable for more than 10 d as indicated by a persistent increase in the transepithelial electrical resistance (TEER) (Figure 1A). The formation of tight junctions was examined by addressing the distribution of Zonula occludens-1 (ZO1; Figure 1B) in cells grown in the Transwell system. ZO-1 decorated the cell–cell contacts, indicating tight junction formation. Together these observations demonstrate that this NHC Transwell culturing system is a suitable model for comparing EVs released from the apical or basolateral surfaces.

sEVs are released from NHCs grown in Transwell culture system

After NHCs had formed a restrictive layer (as assessed by TEER), these Transwell cultures were incubated in EV-depleted media for

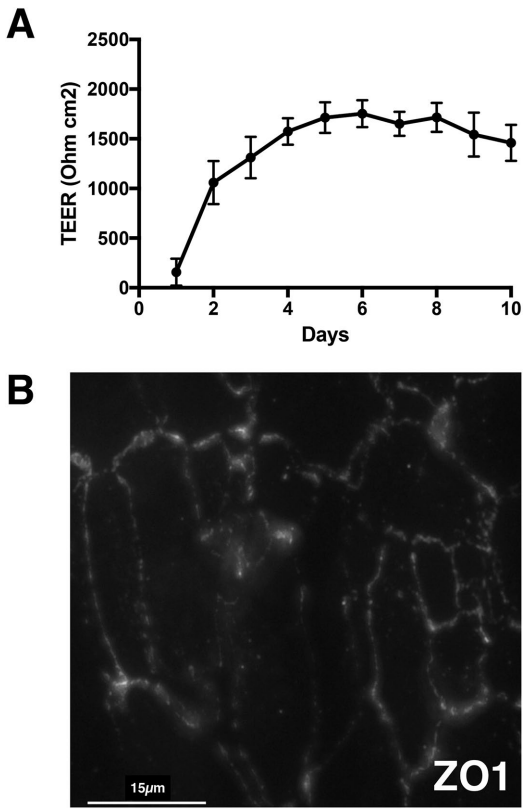

FIGURE 1: Validation of polarized cholangiocyte Transwell culture system. (A) Transepithelial electrical resistance (TEER) was assessed to evaluate the formation of confluent NHC monolayers and the restricted current flow across the monolayer. Resistance is expressed as ohms•cm^2. (B) Immunofluorescence staining of NHC Transwell cultures for Zonula occludens-1 (ZO1) indicated the formation of tight junctions between NHC cells grown in the Transwell culture system.

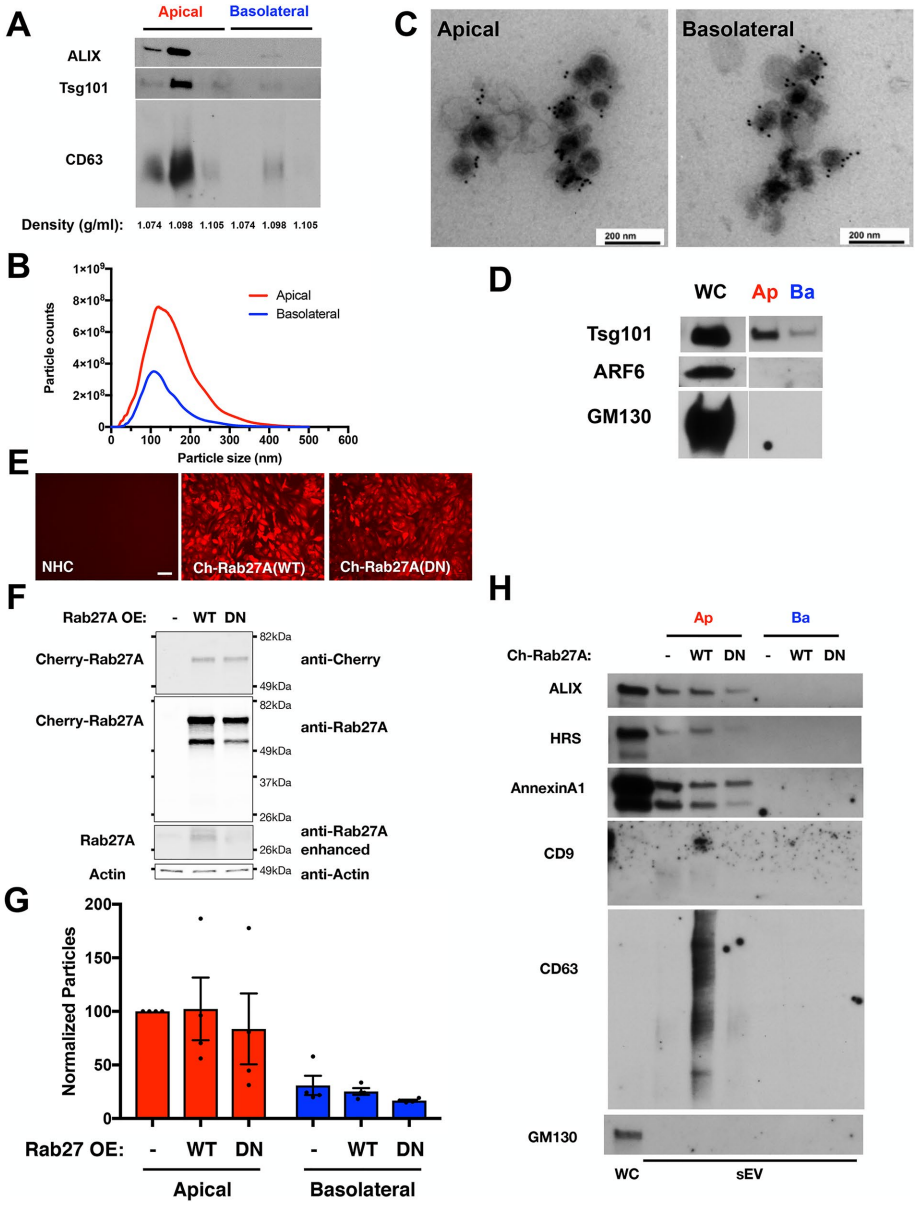

FIGURE 2: Polarized NHC release sEV particles from both apical and basolateral domains. (A) Western blotting equal volumes of apical and basolateral flotation fractions near the 10–20% interface for ESCRT components ALIX and Tsg101 and tetraspanin CD63 indicated peak reactivity in the 1.098 g/ml density fraction. (B) Size distribution resulting from NTA of the small EV fraction isolated from apical and basolateral conditioned media. Apical and basolateral EVs exhibit similar size distributions, and these profiles are consistent with exosome and small microvesicle particle enrichment. (C) Immunoelectron microscopy was performed with apical and basolateral EVs and antibody against the sEV marker CD63. Particles of sizes consistent with sEV and reactive with CD63 were observed in the EV fraction isolated from apical and basolateral conditioned media. (D) Western blotting equal volumes of apical and basolateral small EV fractions was performed with antibodies that detect markers of exosomes (Tsg101), microvesicles (Arf6), or Golgi (GM130). Whole cell extract (WC) was loaded as a positive control for immunodetection in addition to equal volumes of the apical (Ap) and basolateral (Ba) EV fractions. (E) Micrographs of NHC cell lines overexpressing Cherry-Rab27A wild type or dominant negative (DN, T21N), indicating expression in the majority of cells. Scale bar indicates 100 μm. (F) Western blots of NHC cell lines overexpressing Cherry-Rab27A wild type or dominant negative (DN, T21N), indicating enhanced expression. Endogenous Rab27A (darker exposure) and actin are indicated as loading controls. (G, H) Analysis of particles isolated from apical and basolateral conditioned media from NHC cell lines overexpressing Cherry-Rab27A wild type or dominant negative (DN, T21N). NTA (G) indicates reductions in apical (p value <0.05, paired t test) and basolateral (p value <0.05, unpaired t test) sEV numbers with Rab27A(DN) expression. Western blotting (H) indicates Rab27A(DN) reductions in ESCRT components ALIX and HRS and tetraspanin CD63 while the microvesicle marker AnnexinA1 was not impacted. The Golgi marker GM130 is presented as a control for contamination of the EV isolation.

24 h. Conditioned media from the apical and basolateral surfaces were collected for EV isolation, implementing a protocol that favors particles with the density of exosomes/sEVs, and several observations support the conclusion that exosome/sEV enrichment was achieved. First, the migration of the apical and basolateral EVs in the flotation density gradients near the 10–20% interface (~1.098 g/ml), as detected by Western blotting for ESCRT components ALIX and Tsg101 and tetraspanin CD63 (Figure 2A; equal volumes of apical and basolateral fractions), was consistent with exosomes/sEVs (Kowal *et al.*, 2016; Shurtleff *et al.*, 2016; Jeppesen *et al.*, 2019). Second, nanoparticle tracking analysis (NTA) revealed that the size distributions of particles released from apical and basolateral surfaces were both similar to one another and consistent with the reported size of exosomes and small microvesicles (Figure 2B). Third, immunoelectron microscopy with antibodies against the sEV marker, CD63, identified immunoreactive vesicles in both the apical and basolateral EV fractions (Figure 2C). Fourth, Western blotting for ESCRT components ALIX and Tsg101 and tetraspanin CD63 identified these sEV markers in both the apical and basolateral EV fractions (Figure 2, A and D), whereas the Golgi protein GM130 and GTPase Arf6, a microvesicle marker, were not similarly detected (Figure 2D; equal volumes of apical and basolateral fractions). However, a more sensitive indicator of microvesicles, the phospholipid-binding protein AnnexinA1 (Jeppesen *et al.*, 2019), was detected in the EV fractions (Figure 2H; also see Figure 5F later in this article). These observations regarding the size and density of the EV particles and the presence of markers Tsg101, ALIX and CD63, as well as the design of our EV isolation procedure to exclude apoptotic bodies, indicated that polarized NHCs grown in the Transwell culture system release EVs displaying exosome characteristics from both the apical and basolateral domains although small microvesicles are also present. Rab27A promotes MVE fusion with the plasma membrane to release exosomes (Bobrie *et al.*, 2012). To support the conclusion that exosomes contribute to the NHC apical and basolateral sEV populations, a dominant negative form

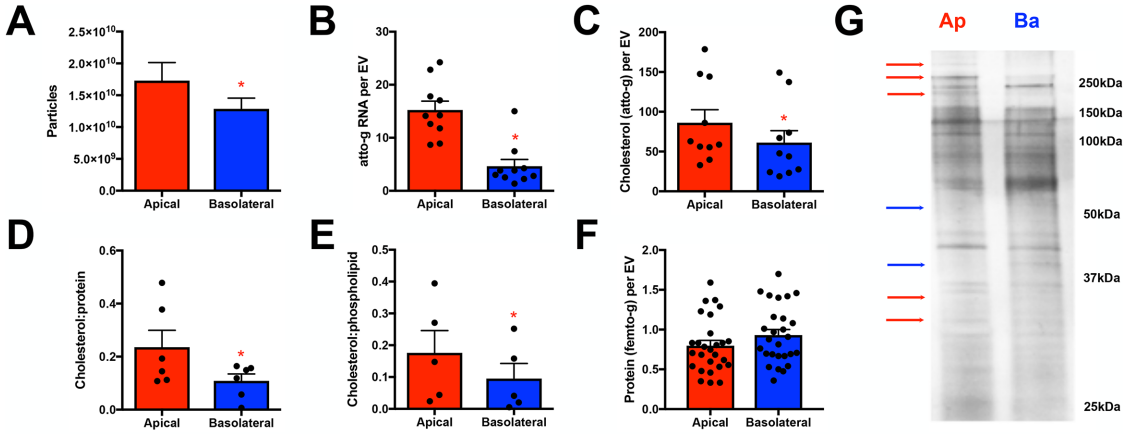

FIGURE 3: Apical and basolateral small EV fractions exhibit differences in number and contents. (A) NTA total counts of small EV fraction particles isolated from the apical and basolateral conditioned media revealing that a greater number of particles within the apical chamber of polarized NHCs was apparent ($n = 24$, p value <0.05). (B) Total RNA concentration was assessed following isolation of RNA from equal numbers of apical and basolateral small EVs. Apical EV RNA content was elevated relative to basolateral EV RNA content ($n = 10$, p value <0.0001). (C–E) Cholesterol level was assessed and normalized to EV number (C), protein level (D), or phospholipid level (E). Apical EVs exhibited increased cholesterol per EV ($n = 10$, p value <0.02) and increased cholesterol:protein ($n = 6$, p value <0.03) and cholesterol:phospholipid ($n = 5$, p value <0.04) ratios. (F) Protein concentration was assessed and normalized to EV number ($n = 27$). (G) Extracts generated from equal numbers of apical and basolateral EVs were resolved by SDS–PAGE and silver stained. A number of species enriched in the apical (red) or basolateral (blue) EV samples are indicated for the purpose of illustration.

of Rab27A (Rab27A T21N) was overexpressed in polarized NHC (Figure 2, E and F). Rab27A(T21N) expression reduced isolation of apical and basolateral sEVs by 28 and 34%, respectively, compared with NHC overexpressing wild-type Rab27A (Figure 2G; p values <0.05). This alteration in sEV numbers with expression of Rab27A(T21N) correlated with reduced levels of ESCRT components ALIX and HRS and tetraspanin CD63 in the apical EV fraction, compared with wild-type Rab27A overexpression, whereas the microvesicle marker AnnexinA1 was largely unaffected (Figure 2H; equal volumes of apical and basolateral fractions); detection of these markers in the basolateral fraction was not achieved in these experiments. These results on particle release and markers support the conclusion that exosomes contribute to the NHC apical and basolateral sEV populations. However, we acknowledge the presence of small microvesicles and will refer to this exosome-containing EV fraction as sEVs.

sEVs released from apical and basolateral domains differ in number and in protein and miRNA contents

Additional analyses at higher resolution revealed several distinctions between these two sEV populations. First, a greater number of sEVs was present in the apical fraction compared with the basolateral fraction (Figures 2B and 3A; p value <0.05). Second, apical sEVs exhibited greater RNA and cholesterol content, with greater cholesterol:protein and cholesterol:phospholipid ratios (Figure 3, B–E). Third, while the protein contents of apical and basolateral sEVs were similar (Figure 3F), silver staining of solubilized apical and basolateral sEVs, normalized for particle number, indicated that even at this resolution some protein species existed at distinct levels within the apical and basolateral sEVs (Figure 3G; normalized to sEV particle number).

To further explore differences in apical and basolateral sEV RNA content, miRNA profiling was performed using a FireFly Bioworks panel, indicating varied enrichment between the apical and basolateral sEVs (Figure 4A; analysis normalized to sEV particle number). Apical enrichment was the predominant pattern with 50 of 65 miRNAs queried exhibiting more than 70% apical release, including miR-34a (97%). Other miRNA species exhibited basolateral enrichment, including miR223 with 62% basolateral release. To validate observed differences in miRNA distribution, QPCR analysis was performed on candidate apical and basolateral miRNAs using normalized numbers of sEVs. These results were consistent with the profiling studies: 83% of miR34a was present in apical sEVs (p value <0.0001), 57% of miR-486 was present in apical sEVs (p value <0.01; compared with 59% apical release in profiling analysis), and 77% of miR223 was present in basolateral sEVs (p value <0.02, Figure 4B, normalized to sEV particle number). In total, our analyses revealed differences between apical and basolateral sEVs with respect to their numbers as well as cholesterol, protein, and RNA contents - both generally and in regard to specific miRNAs. These differences support the hypothesis that polarized NHCs release distinct subpopulations of apical and basolateral sEVs.

Perturbation of N-SMase and the ESCRT component ALIX impact NHC sEV release differently

While previous work has suggested that distinct cellular machinery may be responsible for the biogenesis of subpopulations of ILVs (e.g., ESCRTs, ceramide, tetraspanins) (Mathieu *et al.*, 2019), the manner(s) in which these factors contribute to distinct subclasses of ILVs and how these subclasses relate to exosomes/sEVs are not well understood. Pharmacological inhibition of N-SMase1 was used to examine the contributions of the ceramide pathway to polarized sEV release. Treatment of polarized NHCs with the N-SMase1 inhibitor GW4869 (10 μM) decreased both apical and basolateral sEV release, as observed by NTA (Figure 5A; p value <0.05) and levels of ESCRT component Tsg101 (Figure 5, B and C; equal volumes of apical and basolateral fractions, p value <0.0005 and <0.05, respectively). ESCRT contributions were examined by depletion of the ESCRT-associated factor ALIX. Genetic perturbation was implemented via doxycycline-induced depletion of ALIX in the ALIX.19 NHC clone subsequent to formation of a restrictive polarized

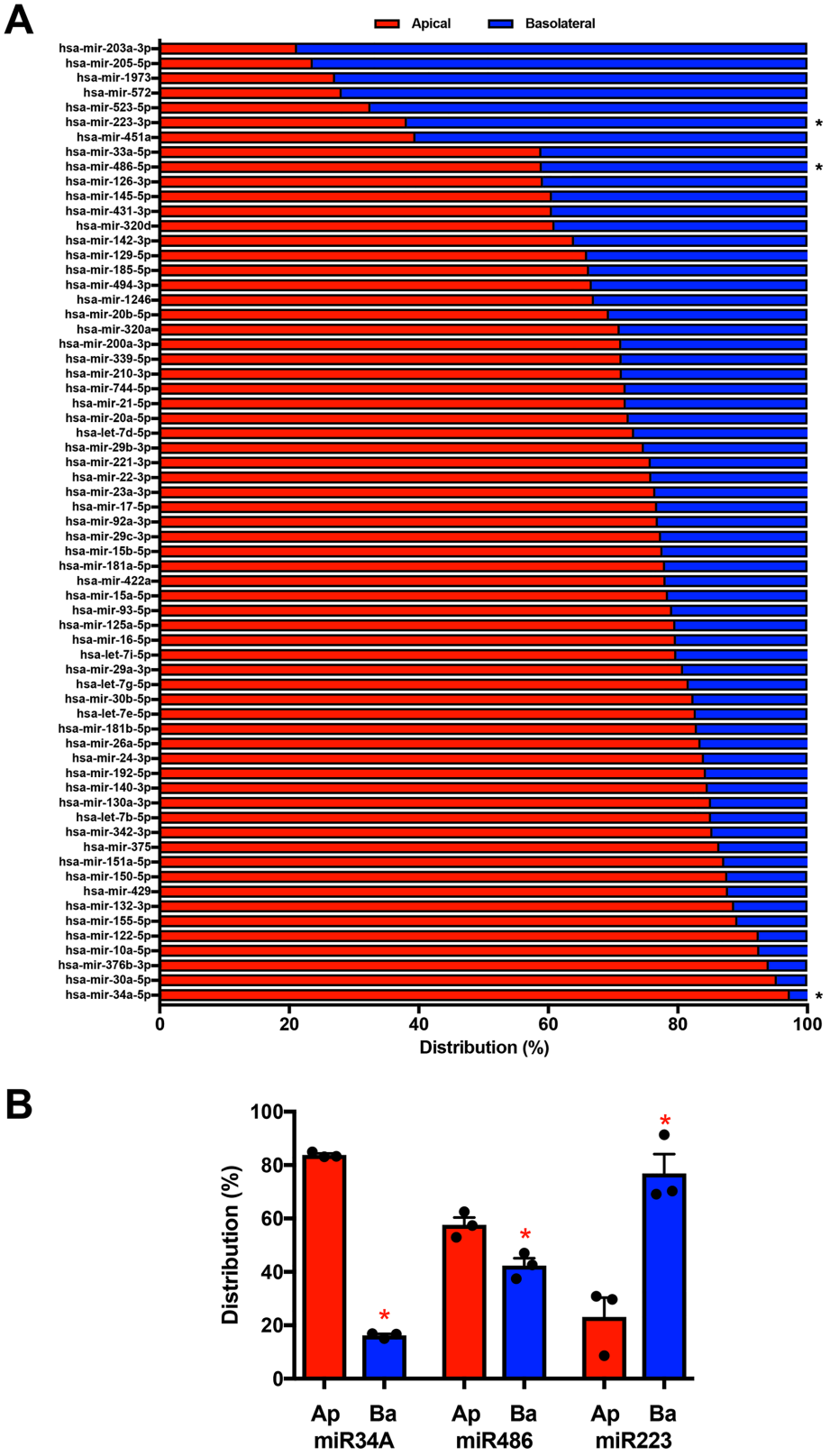

FIGURE 4: Apical and basolateral small EV miRNA contents differ. (A) miRNA profiling of the small EV fractions was performed using the BioWorks FireFly system, and the distribution of miRNA species between the apical (red) and basolateral (blue) EVs is presented. Asterisks indicate mRNA species further examined by QPCR in B. (B) Distributions of three miRNAs exhibiting differential enrichment by profiling were assessed by QPCR. miR34A exhibited apical enrichment ($n = 3$, p value <0.0001), miR486 exhibited weak apical enrichment ($n = 3$, p value <0.01), and miR223 exhibited basolateral enrichment ($n = 3$, p value <0.02).

monolayer (Figure 5D). Doxycycline addition alone did not significantly alter apical or basolateral sEV release in the parental NHC cell line (Figure 5E). In contrast, doxycycline-induced ALIX depletion reduced basolateral sEV levels as indicated by NTA (Figure 5F; p value <0.05); however, apical sEV levels were not similarly reduced, even showing a tendency toward an increase. Western blotting was performed to further examine the sEV fraction. ALIX depletion enhanced ESCRT component Tsg101 levels in the apical sEV fraction (Figure 5, G and H; equal volumes of apical and basolateral fractions; p value <0.005) along with increases in AnnexinA1 and tetraspanin CD9. In contrast, ALIX depletion reduced apical sEV levels of ESCRT component HRS and tetraspanin CD63 (Figure 5G). These results suggest that ALIX depletion induced a change in apical sEV content through increased small microvesicles but reduced exosome release. Together, these results support the conclusions that N-SMase1 contributes to the biogenesis and/or release of both populations of sEVs, while ALIX impacts sEV release in a domain-specific manner.

Apical and basolateral NHC exosomes differentially affect target cells

A functional prediction of the model is that apical and basolateral sEVs will elicit distinct effects within target cells. To test this prediction, sEV-induced signaling in apical and basolateral target cell models was examined. Polarized NHC cells stimulated via the apical surface, mimicking exosome delivery via the bile duct, served as the apical target cell model (in this case modeling cholangiocyte–cholangiocyte communication). Signal transduction in polarized NHC target cells was assessed 24 h subsequent to treatment with equal numbers of apical or basolateral sEVs. This analysis revealed a pattern in which apical sEVs stimulated signal transduction factors in polarized NHCs in a manner distinct from basolateral sEVs (Figure 6A, stimulation with equal numbers of apical or basolateral sEVs; p value <0.0001), with greater activation observed in response to apical sEVs in all cases. sEV-induced signaling was also examined in the human monocyte THP-1 cell line (Tsuchiya *et al.*, 1980) as a basolateral target cell modeling cholangiocyte to liver-resident macrophage communication. In this context, basolateral sEVs stimulated signal transduction factor activation in a manner distinct from apical sEVs (Figure 6B, stimulation with equal numbers of apical or basolateral sEVs; p value <0.01), with greater activation observed in response to

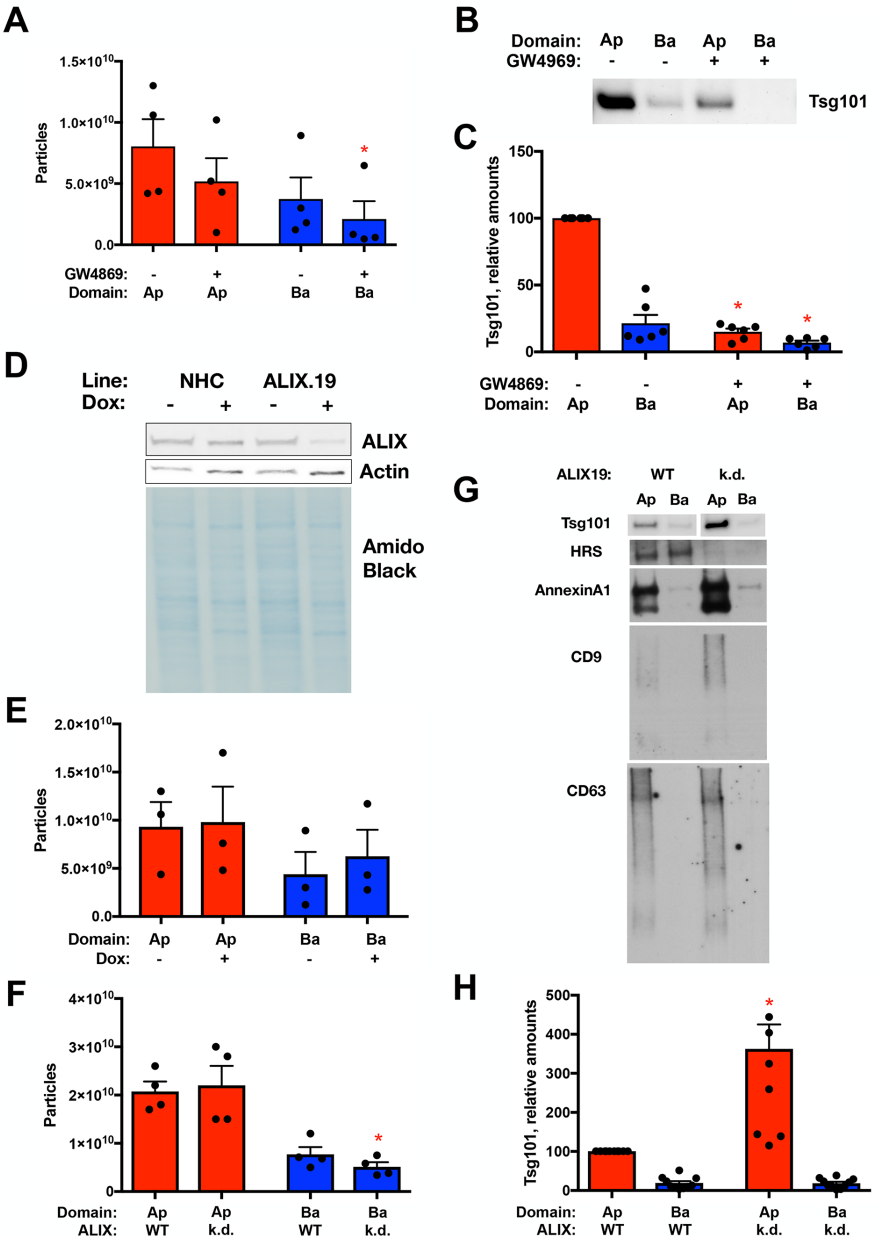

FIGURE 5: Inhibition of N-SMase1 and depletion of ALIX exhibit different effects on polarized sEV release. (A–C) sEV release following treatment of polarized NHC with the N-SMase1 inhibitor GW4869 (10 μM) was assessed by NTA (A) and Western blotting for the ESCRT component Tsg101 loading equal volumes of the sEV fractions. (B, C) GW4869 treatment reduced basolateral EV particle numbers ($n = 4$, p value <0.05) and reduced Tsg101 levels in both the apical and basolateral EV fractions ($n = 6$, p value <0.0005 and <0.05, respectively). (D–H) sEV release following depletion of ALIX from polarized NHC. (D) Doxycycline-induced depletion in the ALIX.19 cell line was assessed by Western blotting for ALIX after 3 d treatment of polarized cells. Actin and amido black staining are presented as loading controls. (E) NTA of sEV release following doxycycline treatment of the parental NHC cell line, indicating similar release independent of treatment. (F–H) sEV release following depletion of ALIX from polarized NHC via doxycycline treatment was assessed by NTA (F) and Western blotting for the ESCRT components Tsg101 and HRS, the microvesicle marker AnnexinA1, and tetraspanins CD63 and CD9 loading equal volumes of the sEV fractions. (G, H). ALIX depletion reduced basolateral EV particle numbers ($n = 4$, p value <0.05) and increased Tsg101 levels in the apical EV fraction ($n = 7$, p value <0.005), correlating with increases in CD9 and AnnexinA1 in the apical sEV fraction.

basolateral sEVs. These results indicated that the apical and basolateral sEVs pools have different signaling capacity toward apical and basolateral target cell models.

The THP-1 basolateral target cell model was further used to assess whether the altered sEV release observed with depletion of the ESCRT-associated factor ALIX impacted polarized sEV communication. While treatment of THP-1 with apical and basolateral sEVs collected from wild-type (WT) NHCs resulted in Akt activation similar to the profile observed using the PathScan Intracellular Signaling Array (Figure 6, C, stimulation with equal volumes of apical or basolateral sEV fraction, and B, stimulation with equal numbers of apical or basolateral sEVs). In contrast, apical sEVs released upon ALIX depletion induced greater Akt activation than either WT NHC apical sEVs or ALIX-depletion basolateral sEVs (Figure 6C; p value <0.05 and 0.05, respectively). This result indicated that ALIX depletion alters polarized sEV communication, consistent with impacts on both the numbers and contents of domain-specific sEV release.

DISCUSSION

While differential EV release from polarized epithelia has been described (van Niel *et al.*, 2001; Tauro *et al.*, 2013; Ji *et al.*, 2014; Chen *et al.*, 2016; Klingeborn *et al.*, 2017; Chin *et al.*, 2018), the contributions of cellular machinery to this process and the signaling impacts of different pools of sEVs remain understudied. We hypothesized that as epithelia, polarized cholangiocytes release distinct sEV pools to mediate signaling via their apical and basolateral surfaces to distinct target cell populations. EV isolation and characterization supports the interpretation that apical and basolateral EV pools contain both exosomes and small microvesicles—collectively "small EVs" —that exhibit differential signaling capacities.

The impacts of dominant negative Rab27A, ALIX depletion, and nSMaseI inhibition on sEV release suggest that MVE biogenesis contributes to formation of the two sEV populations. Two general models of MVE sorting for the secretion of distinct pools of apical and basolateral exosomes can be imagined: 1) a common endosomal compartment whereon different domains generate distinct ILVs and MVEs that are directed to the apical and basolateral membranes to secrete distinct pools of apical and basolateral exosomes; or 2) distinct apical and basolateral endosomal compartments serving as sites for MVE formation, and fusion of the apical and basolateral MVEs with their respective membranes releasing the different pools of exosomes (Figure 7 presents only the second scenario for simplicity). Analysis of rat hepatocyte apical and basolateral plasma membrane composition has demonstrated apical enrichment of cholesterol, evident as

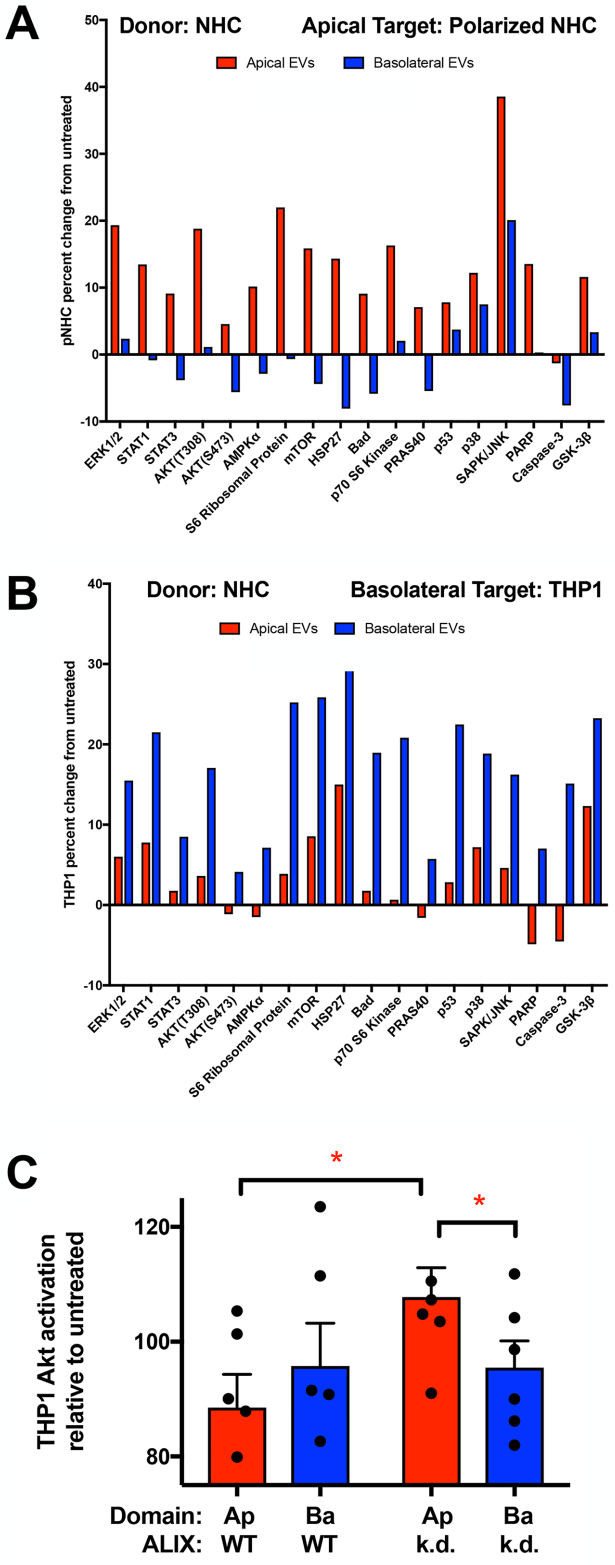

FIGURE 6: Apical and basolateral EVs induce different signaling in apical and basolateral target cells. (A, B) Equal numbers of NHC-derived apical and basolateral sEVs were used to treat (A) polarized NHCs via the apical surface (apical target cell model) or (B) the human monocyte THP1 cell line (basolateral target cell model). Lysates were generated at 24 h, and signaling was assessed using the PathScan Intracellular Signaling Array and normalized to untreated samples. Apical sEVs induced greater activation in this apical target cell model (p value <0.0001), and basolateral sEVs induced greater activation in this basolateral target cell model (p value <0.01). (C) THP1 cells were treated with equal volumes of sEV fractions derived from NHC or ALIX-depleted ALIX.19 cells, lysates were generated at 24 h, and signaling was assessed by Western blotting for Akt activation and normalized to untreated control sample. Apical sEVs from ALIX-depleted cells induced greater Akt activation in this basolateral target cell model than either NHC-derived apical sEVs ($n = 5$, p value <0.05) or basolateral sEVs derived from ALIX-depleted cells. ($n = 5$, p value = 0.05).

increased cholesterol:protein and cholesterol:phospholipid ratios (Mazzone *et al.*, 2006). Polarized cholangiocyte apical sEVs were also enriched in cholesterol compared with basolateral sEVs (Figure 3, D and E); this similarity is consistent with the idea that the membrane sources for apical and basolateral sEVs, including exosomes, are maintained separately. Although we cannot separate the relative contributions of small microvesicles and exosomes in this analysis, the second model is consistent with our analysis and appears to be a simpler mechanism. Further work is required to definitively address the biogenesis of the apical and basolateral sEVs, but our results suggest that some machinery may be common to both pathways while other machinery may be unique. Inhibition of N-SMase with GW4869 to reduce ceramide production decreased both apical and basolateral sEV release (Figure 7, middle panel), but depletion of ALIX reduced basolateral sEV release, altered apical sEV contents, and altered sEV-induced activation of THP1 cells. The effects of ALIX depletion on apical sEV levels of Tsg101, AnnexinA1, and CD9 (increased) versus HRS and CD63 (reduced) suggest that loss of ALIX inhibits apical exosome biogenesis but increases apical microvesicle shedding (Figure 7, right panel). While disruption of ESCRT function through expression of dominant negative Vps4 disrupts both exosome and microvesicle secretion (Jackson *et al.*, 2017), our results suggest that ALIX depletion differentially impacts these ESCRT-mediated EV biogenesis pathways, contributing to the apical sEV pool. Our analyses do not separate defects in MVE formation from MVE trafficking and fusion with the plasma membrane to release exosomes. While the results do not eliminate the possibility that ALIX depletion or N-SMase treatment impacts additional parameters relevant to EV-mediated signaling, the simplest interpretation is that both ALIX depletion and N-SMase inhibition disrupt the biogenesis of MVEs given their roles in the biogenesis of ILVs. Regardless, the differential effects of ALIX depletion and N-SMase inhibition suggest that some machinery is common to biogenesis of the apical and basolateral sEV populations while other factors are distinct.

The differential signaling capacity of apical and basolateral sEVs could be mediated both by factors present on the surface of the particles as well as factors contained within the particles. While we observed differences between apical and basolateral sEV-induced signaling at 24 h, we did not observe measurable sEV-induced signaling following 1-h treatment (unpublished data). This discrepancy may indicate that the difference in internal contents (e.g., miRNAs) between apical and basolateral sEVs is a major factor driving the observed differential signaling capacity. Alternatively, the surface components of the two populations may direct more effective delivery of apical or basolateral sEV contents to generate differential effects, and this issue needs to be explored in future studies. An appealing mechanism for the differential signaling effect of the two sEV populations is the different repertoire of miRNA species present in each. A number of mechanisms have been described for the secretion of miRNAs in EVs in nonpolarized cells (e.g., hRNPA2, YBX1, YBX2) (Villarroya-Beltri *et al.*, 2013; Shurtleff *et al.*, 2016), but the

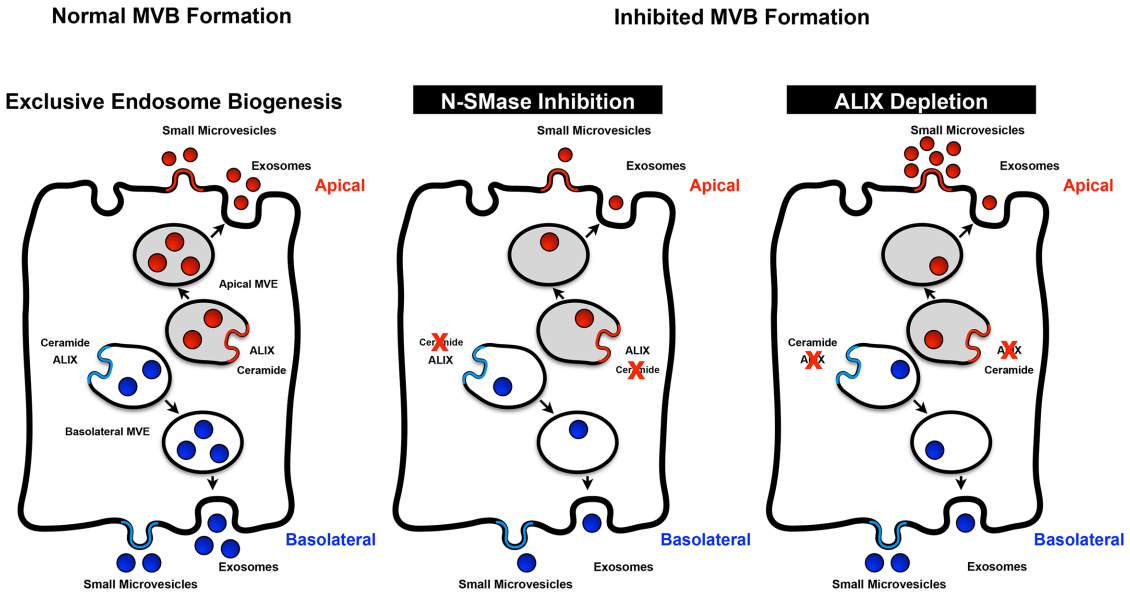

FIGURE 7: Exclusive MVE biogenesis model. (Left) The sorting of exosome cargoes into MVEs occurs on distinct apical and basolateral endosomes, which then fuse with their respective plasma membrane domains to release the apical and basolateral exosomes. These exosomes along with small microvesicles shed from the plasma membrane comprise the sEV population. (Middle) Inhibition of the ceramide pathway via GW4869 treatment perturbed both the apical and basolateral sEV populations. (Right) In contrast, ALIX depletion reduced the numbers of basolateral sEVs released and altered the apical sEVs with respect to their contents and signaling capacity through reducing exosome secretion but enhancing small microvesicle shedding.

mechanisms by which specific miRNAs are sorted into apical or basolateral sEVs are unclear. If these known factors are contributing to miRNA secretion in a polarized manner, the question of how these cytosolic factors themselves are selectively sorted into apical or basolateral exosomes/sEVs will be interesting to resolve. Altered miRNA levels in plasma/serum, bile, or urine have been identified as potential biomarkers in cholangiocarcinoma, biliary atresia, primary sclerosing cholangitis, and primary biliary cholangitis (reviewed in Olaizola *et al.*, 2018), and a number of these miRNAs (e.g., miR122-5p, 90% apical; miR21-5p, 72% apical; miR200a-3p, 65% apical) exhibited polarized release in sEVs in our NHC system. While differential expression in diseased cholangiocytes is one mechanism that could alter levels of these biomarkers, perturbation of polarized sEV release during disease progression may also contribute to changes in their abundance in different biological fluids. Further understanding how polarized exosome/sEV release is modulated in cholangiopathies may provide important insights into disease pathogenesis. Herein we have established an in vitro system for studying polarized cholangiocyte sEV release and communication. This system will be useful to further assess polarized cell–cell communication in the cholangiopathies and in other diseases involving epithelial cells, including alterations in the contents of these particles and changes in the signaling capacities of apical and basolateral sEVs.

In addition to its role in exosome biogenesis, the ESCRT machinery mediates membrane remodeling in a number of important cellular processes including the formation of MVEs during receptor down-regulation (Katzmann *et al.*, 2001, 2002; Bache *et al.*, 2004a; Shim *et al.*, 2006; Sierra *et al.*, 2010; Giordano *et al.*, 2011; Hislop *et al.*, 2011; Ma *et al.*, 2015; Parkinson *et al.*, 2015; Christ *et al.*, 2017; Schoneberg *et al.*, 2017), abscission of the cellular bridge during cell division (Carlton and Martin-Serrano, 2007; Elia *et al.*, 2011; Guizetti *et al.*, 2011; Lafaurie-Janvore *et al.*, 2013; Mierzwa and Gerlich, 2014; Mierzwa *et al.*, 2017), and the closure of the autophagic membrane during autophagy (Takahashi *et al.*, 2018). Defects in ESCRT function have been associated with the development of neurological disease (frontotemporal dementia, CHMP2B) (Skibinski *et al.*, 2005), cataracts (autosomal dominant cataracts, CHMP4B) (Shiels *et al.*, 2007), and cancer (tumor suppression, HD-PTP) (Bache *et al.*, 2004b; Mattissek and Teis, 2014; Manteghi *et al.*, 2016). These disease processes have generally been considered to result from the cell autonomous defects in ESCRT function (e.g., perturbations in receptor trafficking and signaling, autophagy, aneuploidy, and membrane repair). Our results indicate that perturbation of ESCRT function, in this case through ALIX depletion, can also impact intercellular communication by altering polarized sEV release from donor cells. These results suggest that the role of ESCRTs in disease should be considered with respect to altered exosome communication in addition to cell autonomous defects in future studies.

MATERIALS AND METHODS

Cell lines and cell culture

Low-passage NHCs (Joplin *et al.*, 1989) were cultured in a manner similar to that previously described (Banales *et al.*, 2012; Tabibian *et al.*, 2014) in 5% CO_2, normal oxygen in modified H69 media (DMEM/F12 [Life Technologies 11330-032], 10% fetal bovine serum [FBS], 1× penicillin/streptomycin [Life Technologies 15140-122], 24.3 µg/ml adenine [Sigma A8626], 5 µg/ml insulin [Sigma I-6634], 1 µg/ml epinephrine [Sigma E-1635], 8.3 µg/ml transferrin [Sigma T-1147], 2.27 ng/ml triiodo-L-thyronine [Sigma T-6397], 0.267 µg/ml hydrocortisone [Sigma H-0888]). FBS used included heat-inactivated FBS (Sigma F4135), tetracycline negative FBS (Corning 35-075-CV; Takara 631106), and exosome-depleted FBS (Life Technologies A25904/A27208) as appropriate. Mycoplasma contamination was monitored using the Mycoplasma Detection Kit (SouthernBiotech 13100-01). NHC were cultured using collagen Type I (Corning 354236)-coated tissue culture plastic ware or collagen-coated

Transwell supports with 0.4 µm polycarbonate membrane (7.5 cm insert: Corning 3419; 12 mm insert, 12 well: Corning 3401). NHC cell lines overexpressing Rab27A wild type or dominant negative (T21N) were generated by infecting NHC with pHR-SIN-CSGWΔNotI containing fused mCherry-C3 and human Rab27A coding sequences, with the T21N mutation introduced by site-directed mutagenesis using the GeneTailor Site-Directed Mutagenesis System (ThermoFisher Scientific); all plasmids were sequenced to validate construction; validation of cell lines was performed by Western blotting with Living Colors mCherry monoclonal antibody (Clontech 632543), Rab27A D7Z9Q monoclonal antibody (Cell Signaling Technology 69295) and β-actin monoclonal antibody (Sigma A5441) along with IRDye680LT goat anti-rabbit immunoglobulin G (IgG) or goat anti-mouse IgG (Li-Cor 926-68021 and 926-68020) secondary antibodies and detection with the Odyssey Infrared Imager with ImageStudio software (Li-Cor). The ALIX.19 subclone was generated by infecting NHC with TRIPZ Human PDCD6IP shRNA (Dharmacon V2THS_357893) lentivirus and selecting for puromycin (Sigma P9620) resistance. The ALIX.19 colony was selected, cultured, and characterized for doxycycline (Takara 631311)-induced ALIX depletion and exosome secretion; the validation of the cell line was performed by Western blotting with ALIX (Cell Signaling Technology 92880) and β-actin monoclonal antibody, along with IRDye680LT goat anti-rabbit IgG or goat anti-mouse IgG secondary antibodies, and detection with Odyssey Infrared Imager with ImageStudio software. A second clone, ALIX.26, displayed similar doxycycline-induced ALIX depletion and altered exosome secretion (unpublished data). GW4869 (Sigma D1692) treatment was 10 µM for 24 h. The human monocytic cell line THP-1 (Tsuchiya *et al.*, 1980) (ATCC TIB-202) was cultured as previously described (Hirsova *et al.*, 2016a) in 5% CO_2, normal oxygen in RPMI-1640 with 10% FBS and 0.05 mM 2-mercaptoethanol.

Immunofluorescence

Low-passage NHC (1e5) were plated in 12 mm insert, 0.4 µm PC membrane Transwells in modified H69 media with heat-inactivated FBS. Cells were cultured for 8 d, and TEER was measured using the Millicell-ERS Volt-Ohm Meter (Millipore MERSSTX01) to ensure formation of confluent, restrictive monolayer. Samples were then washed with phosphate-buffered saline (PBS) and fixed (100 mM PIPES, pH 6.95, 1 mM ethylene glycol-bis(2-aminoethylether)-*N*,*N*,*N*′,*N*′-tetraacetic acid, 3 mM $MgSO_4$, 2.5% formaldehyde) for 20 min at 37°C. Cells were permeabilized with 0.1% Triton X-100, blocked in 5% goat serum, and probed with rabbit ZO-1 D6L1E monoclonal antibody (Cell Signaling Technology 13663) and Alexa568-goat anti-rabbit secondary antibody (ThermoFisher A-11011). The membrane was excised from the Transwell support and mounted using ProLong Gold Antifade Mountant with 4′,6-diamidino-2-phenylindole (ThermoFisher P36935). Samples were imaged as Z-stacks using a DeltaVision deconvolution system (Applied Precision, Issaquah, WA) with an Olympus IX70 fluorescence microscope (Center Valley, PA) and CoolsnapHQ digital camera (Photometrics, Tucson, AZ), and micrographs were deconvolved and projected using the Softworx 3.5.1 software package (Applied Precision).

EV isolation and characterization

Totals of 4e6 low-passage NHC, NHC Cherry-Rab27A WT, NHC Cherry-Rab27A T21N, or ALIX.19 were plated in collagen-coated 7.5 cm insert, 0.4 µm polycarbonate membrane Transwell plates in modified H69 media with heat-Inactivated FBS or tetracycline-negative FBS and cultured for 3 d. TEER was measured to ensure formation of a confluent, restrictive monolayer. Cells were washed with Dulbecco's PBS (DPBS) (Corning 21-031-CV) and incubated for 24 h in H69 media with exosome-depleted FBS. Media from the apical and basolateral chambers were collected, and cells were refed with H69 media with exosome-depleted FBS with the addition of 1 µg/ml doxycycline. Media incubation and collection for exosome isolation were then repeated for up to 4 d. For inhibition of N-SMase, after the initial 24 media collection, cells were refed with exosome-depleted FBS with the addition of 1 µg/ml doxycycline and 10 µM GW4869. Exosome isolation was performed, subjecting the entire volume of apical and basolateral collected media to spins at 500 × *g* for 10 min and then 3000 × *g* for 30 min. Cleared media was then either filtered through a 0.2 µm membrane or spun at 30,000 × *g* for 30 min. Small EVs were then collected on 60% sucrose or iodixanol overlaid with 10% sucrose or iodixanol via 200,000 × *g* spin for 2 h in a SW28 or SW41 rotor. The 10–60% interface was collected, resuspended to greater than 40% sucrose or iodixanol, overlaid with 40%, 20%, and 10% sucrose and PBS or 40%, 30%, 20%, and 10% iodixanol and PBS, and spun for more than 12 h at 200,000 × *g* in a SW41 rotor, similar to the procedure described in Kowal *et al.* (2016) and Shurtleff *et al.* (2016). Harvest of the flotation density gradient fractions indicated migration of EVs at the 10–20% sucrose or near the 10–20% iodixanol interface, and these particles were characterized further. Refractive index of flotation fractions was assessed using a Benchtop Refractometer (Milton Roy 334610) and used to determine solution density. All spins were conducted at 4°C, and particles were stored at 4°C.

NTA was performed by diluting EVs in counting buffer (PBS [Corning 21-040-EV], 10 mM sucrose, 1 mM EDTA, filtered through Vivaspin20 10 kDa MWCO [GE Healthcare 28-9323-60]) and analyzing using NanoSight NS300 with NTA 3.0 software (Malvern Instruments) with Camera Capture setting 12, and Process Threshold 3 or 4, internally consistent within each experiment. Samples were run continuously through a flow-cell top-plate using a syringe pump at a rate of 25 µl/min. At least three videos of 60 s documenting Brownian motion of particles were recorded, and a minimum of 1000 valid tracks were analyzed. Prism 7 (GraphPad) was used for analysis, including paired and unpaired *t* tests.

Immunoelectron microscopy was performed by the Mayo Clinic Microscopy and Cell Analysis Core. EV pellets were fixed with 4% paraformaldehyde in 100 mM phosphate buffer and deposited on Formvar/Carbon-coated 200 Mesh Nickle grids. Samples were probed with CD63 primary antibody (Santa Cruz Biotechnology) and/or 10 nm gold-conjugated protein A. Samples were then treated with 1% glutaraldehyde in PBS and stained in 4% uranyl acetate, 2% methylcellulose. Images were collected using the JEOL 1400 electron microscope.

Western blot analysis of EV fraction was performed by combining equal volumes of sample with 5× Laemmli sample buffer. Samples were denatured, resolved on Mini-PROTEAN TGX 4-20% gels (Bio-Rad 456-1096), and transferred to supported nitrocellulose membranes (Bio-Rad 1620094). Western blotting was performed with primary antibodies against Tsg101 (AbCam ab125011), Arf6 (AbCam ab77581), AnnexinA1 (AbCam ab214486), HRS (Cell Signaling Technology15087), ALIX (Cell Signaling Technology 92880), CD9 (Cell Signaling Technology 13174), and GM130 (Cell Signaling Technology 12480) and secondary antibody horseradish peroxidase (HRP)-linked goat anti-rabbit IgG (Cell Signaling Technology 7074; Thermo Fisher G21234). Detection of CD63 was modified by reducing the amount of β-mercaptoethanol in the sample (0 or 12 µM final concentration); Western blotting was performed using the CD63 H5C6 mouse monoclonal antibody (deposited to Developmental Studies Hybridoma Bank (DSHB). The Johns Hopkins University

School of Medicine by J.T. August and J.E.K. Hildreth and maintained by DSHB, created by the National Institute of Child and Human Development of the National Institutes of Health and maintained at the University of Iowa Department of Biology, Iowa City) and secondary antibody HRP-linked goat anti-mouse IgG (Thermo Fisher G21040). The SuperSignal West Femto Maximum Sensitivity Substrate (ThermoFisher 34095) was used in conjunction with autoradiography film or the UVP AutoChemi system (Upland, CA) to develop blots, and ImageQuantTL (GE Life Sciences) and Prism 7 (GraphPad) were used for analysis.

The MicroBCA Assay (ThermoFisher 23235) was used to assess the protein concentration of equal volumes of exosome fractions following removal of sucrose. Protein was extracted with 5% M-PER Mammalian Protein Extraction Reagent (ThermoFisher 78501). The protein concentration was normalized to particle number assessed by NTA. Total lipids were extracted from exosome preps according to the Bligh and Dyer method (Bligh and Dyer, 1959) scaled to accommodate an aqueous volume of 40 µl using 5 × 50 mm disposable culture tubes sealed with Teflon tape. Cholesterol was determined by the method of Amplex Red (ThermoFisher A12216). Phosphate was determined on the extracted samples after acid hydrolysis by the method of Zhou and Arthur (Zhou and Arthur, 1992) using malachite green scaled to a total volume of 120 µl and read on a nanodrop spectrometer using phosphatidylcholine as a standard. The cholesterol concentration was normalized to particle number assessed by NTA, to protein concentration assessed by MicroBCA, and phospholipid concentration assessed by malachite green. RNA was extracted from exosome fractions normalized to particle number using miRCURY RNA Isolation Kit, Cell and Plant (Exiqon 300110) and quantified using the Quant-iT RiboGreen RNA Assay Kit (ThermoFisher R11490). Silver staining of normalized numbers of exosomes was performed using the Silver Stain Plus Kit (Bio-Rad 1610449).

Profiling of miRNAs was performed by submitting equal volumes of apical and basolateral exosome fraction pairs in triplicate to FireFly Bioworks for analysis using the Immunology V2 Panel of 65 miRNAs (AbCam ab218369). This panel was chosen due to interest in how cholangiocyte-derived exosomes might influence the immune system. Validation of differential distribution was performed by quantitative PCR (QPCR) using RNA isolated from equal numbers of exosomes (described above). miR223-3p distribution was assessed using the TaqMan Advanced miRNA cDNA Synthesis Kit (ThermoFisher A28007) in conjunction with TaqMan Universal Master Mix II, no UNG (ThermoFisher 4440043) and TaqMan Advanced MicroRNA Assay (ThermoFisher A25576 477983_mir). miR34a-5p and miR486-5p distributions were assessed using the TaqMan MicroRNA Reverse Transcription Kit (ThermoFisher 4366596) with miR-specific primers in conjunction with TaqMan Universal Master Mix II, no UNG and TaqMan MicroRNA Assays (ThermoFisher 4427975 000426, 001278).

Target cell signaling

To examine the impact of exosomes on an apical target cell model, NHC cells were grown on collagen-coated six-well plates (Corning 3506) 3 d past confluency in modified H69 media with 1 µg/ml doxycycline. Cells were washed with DPBS and serum-starved in DMEM:F12 for 4 h before stimulation with equal numbers of apical or basolateral exosomes (4e8) in DMEM:F12. Cells were washed in cold PBS and lysed in PathScan Sandwich ELISA Lysis Buffer (Cell Signaling Technologies 7018) with the addition of Complete EDTA-free Protease Inhibitor Cocktail Tablet (Roche 04693132001), PhosSTOP Phosphatase Inhibitor Cocktail Tablet (Roche 04906837001), and 100 µM 100 µM AEBSF (Fisher BP2644-100). Protein concentration normalization was performed using Protein Assay Dye Reagent Concentrate (Bio-Rad 5000006), and signaling was evaluated using the PathScan Intracellular Signaling Array (Cell Signaling Technology 7744) using fluorescent detection reagent following the manufacturer's instructions. Signal was analyzed using the Odyssey Infrared Imager with ImageStudio software (LiCor Biosciences, Lincoln, NE) and Prism 7 (GraphPad). Stimulations were performed in triplicate in two independent experiments.

To examine the impact of exosomes on a basolateral target cell model, equal numbers of apical and basolateral exosomes (2e7) were used to treat 1e6 THP-1 cells in RPMI-1640 with 10% FBS and 0.05 mM 2-mercaptoethanol for 24 h in suspension. Cells were then pelleted, washed in cold PBS, and processed as described for examination of signaling in the apical target cell model using PathScan Intracellular Signaling Array with fluorescent detection reagent following the manufacturer's instructions. Stimulations were performed in triplicate in three independent experiments.

To examine the impact of ALIX depletion on exosome signaling, equal volumes of the apical and basolateral exosome fractions released by doxycycline-treated NHC or ALIX.19 cells were used to treat 5e5 THP-1 cells in RPMI-1640 with 10% FBS and 0.05 mM 2-mercaptoethanol for 24 h in suspension. Cells were then pelleted, washed in cold PBS, and lysed in Reverse Phase Protein Array Lysis Buffer (1% Triton X-100, 50 mM HEPES, pH 7.4, 150 mM NaCl, 1.5 mM $MgCl_2$, 1 mM EGTA, 100 mM NaF, 10 mM Na pyrophosphate, 1 mM Na_3VO_4, 10% glycerol, 100 µM AEBSF [Fisher BP2644-100], with Complete EDTA-free Protease Inhibitor Cocktail Tablet [Roche 04693132001] and PhosSTOP Phosphatase Inhibitor Cocktail Tablet [Roche 04906837001]) (Grote *et al.*, 2008). Cleared lysates were combined with 5× Laemmli sample buffer, denatured, resolved by SDS–PAGE, and transferred to nitrocellulose. Western blotting was performed using rabbit anti-phospho-Akt S473 antibody D9E (Cell Signaling Technology 4060) and mouse anti-total Akt antibody 40D4 (Cell Signaling Technology 2920) with goat anti-rabbit IgG 680LT (LiCor 925-68021) and goat anti-mouse IgG 800CW (LiCor 925-32210). Signal was detected using the Odyssey Infrared Imager with ImageStudio software (LiCor) and analyzed using ImageJ (Schneider *et al.*, 2012), ImageQuantTL (GE Life Sciences), and Prism 7 (GraphPad) to calculate the ratio of phospho/total-Akt. Two separate preparations of exosome fractions were used and analyzed for stimulations in four replicate experiments.

ACKNOWLEDGMENTS

We thank the members of the Katzmann and LaRusso laboratories for many helpful suggestions and Bing Huang for his assistance with immunoelectron microscopy. This work was supported by funding from the Mayo Clinic Center for Biomedical Discovery (D.J.K., N.F.L.), the Mayo Clinic Graduate School of Biomedical Sciences (C.N.R., L.C.D.), PSC Partners Seeking a Cure (2017 grant 4, D.J.K.), and the National Institutes of Health (GM116826, D.J.K., supporting B.A.D.; DK57993, N.F.L., supporting L.O.M.; T32 DK07198, supporting L.O.M.; and P30DK084567 supporting the Mayo Clinic Center for Cell Signaling in Gastroenterology Microscopy Core). The content is solely the responsibility of the authors and does not necessarily represent the official views of the National Institutes of Health,

REFERENCES

Al Suraih MS, Trussoni CE, Splinter PL, LaRusso NF, O'Hara SP (2020). Senescent cholangiocytes release extracellular vesicles that alter target cell phenotype via the epidermal growth factor receptor. Liver Int, DOI:10.1111/liv.14569.

Arbelaiz A, Azkargorta M, Krawczyk M, Santos-Laso A, Lapitz A, Perugorria MJ, Erice O, Gonzalez E, Jimenez-Aguero R, Lacasta A, *et al.* (2017).

Serum extracellular vesicles contain protein biomarkers for primary sclerosing cholangitis and cholangiocarcinoma. Hepatology 66, 1125–1143.
Bache KG, Slagsvold T, Cabezas A, Rosendal KR, Raiborg C, Stenmark H (2004a). The growth-regulatory protein HCRP1/hVps37A is a subunit of mammalian ESCRT-I and mediates receptor down-regulation. Mol Biol Cell 15, 4337–4346.
Bache KG, Slagsvold T, Stenmark H (2004b). Defective downregulation of receptor tyrosine kinases in cancer. EMBO J 23, 2707–2712.
Baietti MF, Zhang Z, Mortier E, Melchior A, Degeest G, Geeraerts A, Ivarsson Y, Depoortere F, Coomans C, Vermeiren E, et al. (2012). Syndecan-syntenin-ALIX regulates the biogenesis of exosomes. Nat Cell Biol 14, 677–685.
Banales JM, Huebert RC, Karlsen T, Strazzabosco M, LaRusso NF, Gores GJ (2019). Cholangiocyte pathobiology. Nat Rev Gastroenterol Hepatol 16, 269–281.
Banales JM, Saez E, Uriz M, Sarvide S, Urribarri AD, Splinter P, Tietz Bogert PS, Bujanda L, Prieto J, Medina JF, LaRusso NF (2012). Up-regulation of microRNA 506 leads to decreased Cl-/HCO3- anion exchanger 2 expression in biliary epithelium of patients with primary biliary cirrhosis. Hepatology 56, 687–697.
Bligh EG, Dyer WJ (1959). A rapid method of total lipid extraction and purification. Can J Biochem Physiol 37, 911–917.
Bobrie A, Krumeich S, Reyal F, Recchi C, Moita LF, Seabra MC, Ostrowski M, Thery C (2012). Rab27a supports exosome-dependent and -independent mechanisms that modify the tumor microenvironment and can promote tumor progression. Cancer Res 72, 4920–4930.
Carlton JG, Martin-Serrano J (2007). Parallels between cytokinesis and retroviral budding: a role for the ESCRT machinery. Science 316, 1908–1912.
Chen Q, Takada R, Noda C, Kobayashi S, Takada S (2016). Different populations of Wnt-containing vesicles are individually released from polarized epithelial cells. Sci Rep 6, 35562.
Cheung AC, Lorenzo Pisarello MJ, LaRusso NF (2018). Pathobiology of biliary epithelia. Biochim Biophys Acta 1864, 1220–1231.
Chin AR, Yan W, Cao M, Liu X, Wang SE (2018). Polarized secretion of extracellular vesicles by mammary epithelia. J Mammary Gland Biol Neoplasia 23, 165–176.
Christ L, Raiborg C, Wenzel EM, Campsteijn C, Stenmark H (2017). Cellular functions and molecular mechanisms of the ESCRT membrane-scission machinery. Trends Biochem Sci 42, 42–56.
Colombo M, Raposo G, Thery C (2014). Biogenesis, secretion, and intercellular interactions of exosomes and other extracellular vesicles. Annu Rev Cell Dev Biol 30, 255–289.
Eaton JE, Talwalkar JA, Lazaridis KN, Gores GJ, Lindor KD (2013). Pathogenesis of primary sclerosing cholangitis and advances in diagnosis and management. Gastroenterology 145, 521–536.
Elia N, Sougrat R, Spurlin TA, Hurley JH, Lippincott-Schwartz J (2011). Dynamics of endosomal sorting complex required for transport (ESCRT) machinery during cytokinesis and its role in abscission. Proc Natl Acad Sci USA 108, 4846–4851.
Giordano F, Simoes S, Raposo G (2011). The ocular albinism type 1 (OA1) GPCR is ubiquitinated and its traffic requires endosomal sorting complex responsible for transport (ESCRT) function. Proc Natl Acad Sci USA 108, 11906–11911.
Grote T, Siwak DR, Fritsche HA, Joy C, Mills GB, Simeone D, Whitcomb DC, Logsdon CD (2008). Validation of reverse phase protein array for practical screening of potential biomarkers in serum and plasma: accurate detection of CA19-9 levels in pancreatic cancer. Proteomics 8, 3051–3060.
Guizetti J, Schermelleh L, Mantler J, Maar S, Poser I, Leonhardt H, Muller-Reichert T, Gerlich DW (2011). Cortical constriction during abscission involves helices of ESCRT-III-dependent filaments. Science 331, 1616–1620.
Hanson PI, Roth R, Lin Y, Heuser JE (2008). Plasma membrane deformation by circular arrays of ESCRT-III protein filaments. J Cell Biol 180, 389–402.
Hessvik NP, Llorente A (2018). Current knowledge on exosome biogenesis and release. Cell Mol Life Sci 75, 193–208.
Hirschfield GM, Karlsen TH, Lindor KD, Adams DH (2013). Primary sclerosing cholangitis. Lancet 382, 1587–1599.
Hirsova P, Ibrahim SH, Krishnan A, Verma VK, Bronk SF, Werneburg NW, Charlton MR, Shah VH, Malhi H, Gores GJ (2016a). Lipid-induced dignaling causes release of inflammatory extracellular vesicles from hepatocytes. Gastroenterology 150, 956–967.
Hirsova P, Ibrahim SH, Verma VK, Morton LA, Shah VH, LaRusso NF, Gores GJ, Malhi H (2016b). Extracellular vesicles in liver pathobiology: small particles with big impact. Hepatology 64, 2219–2233.
Hislop JN, Henry AG, von Zastrow M (2011). Ubiquitination in the first cytoplasmic loop of mu-opioid receptors reveals a hierarchical mechanism of lysosomal down-regulation. J Biol Chem 286, 40193–40204.
Jackson CE, Scruggs BS, Schaffer JE, Hanson PI (2017). Effects of inhibiting VPS4 support a general role for ESCRTs in extracellular vesicle biogenesis. Biophys J 113, 1342–1352.
Jeppesen DK, Fenix AM, Franklin JL, Higginbotham JN, Zhang Q, Zimmerman LJ, Liebler DC, Ping J, Liu Q, Evans R, et al. (2019). Reassessment of exosome composition. Cell 177, 428–445.e418.
Ji H, Chen M, Greening DW, He W, Rai A, Zhang W, Simpson RJ (2014). Deep sequencing of RNA from three different extracellular vesicle (EV) subtypes released from the human LIM1863 colon cancer cell line uncovers distinct miRNA-enrichment signatures. PLoS One 9, e110314.
Joplin R, Strain AJ, Neuberger JM (1989). Immuno-isolation and culture of biliary epithelial cells from normal human liver. In Vitro Cell Dev Biol 25, 1189–1192.
Julich-Haertel H, Urban SK, Krawczyk M, Willms A, Jankowski K, Patkowski W, Kruk B, Krasnodebski M, Ligocka J, Schwab R, et al. (2017). Cancer-associated circulating large extracellular vesicles in cholangiocarcinoma and hepatocellular carcinoma. J Hepatol 67, 282–292.
Katzmann DJ, Babst M, Emr SD (2001). Ubiquitin-dependent sorting into the multivesicular body pathway requires the function of a conserved endosomal protein sorting complex, ESCRT-I. Cell 106, 145–155.
Katzmann DJ, Odorizzi G, Emr SD (2002). Receptor downregulation and multivesicular-body sorting. Nat Rev Mol Cell Biol 3, 893–905.
Klingeborn M, Dismuke WM, Skiba NP, Kelly U, Stamer WD, Bowes Rickman C (2017). Directional exosome proteomes reflect polarity-specific functions in retinal pigmented epithelium monolayers. Sci Rep 7, 4901.
Kowal J, Arras G, Colombo M, Jouve M, Morath JP, Primdal-Bengtson B, Dingli F, Loew D, Tkach M, Thery C (2016). Proteomic comparison defines novel markers to characterize heterogeneous populations of extracellular vesicle subtypes. Proc Natl Acad Sci USA 113, E968–E977.
Lafaurie-Janvore J, Maiuri P, Wang I, Pinot M, Manneville JB, Betz T, Balland M, Piel M (2013). ESCRT-III assembly and cytokinetic abscission are induced by tension release in the intercellular bridge. Science 339, 1625–1629.
Larios J, Mercier V, Roux A, Gruenberg J (2020). ALIX- and ESCRT-III-dependent sorting of tetraspanins to exosomes. J Cell Biol 219, e201904113.
Lazaridis KN, LaRusso NF (2016). Primary sclerosing cholangitis. N Engl J Med 375, 1161–1170.
Ma H, Wardega P, Mazaud D, Klosowska-Wardega A, Jurek A, Engstrom U, Lennartsson J, Heldin CH (2015). Histidine-domain-containing protein tyrosine phosphatase regulates platelet-derived growth factor receptor intracellular sorting and degradation. Cell Signal 27, 2209–2219.
Maas SL, Breakefield XO, Weaver AM (2017). Extracellular vesicles: unique intercellular delivery vehicles. Trends Cell Biol 27, 172–188.
Manteghi S, Gingras MC, Kharitidi D, Galarneau L, Marques M, Yan M, Cencic R, Robert F, Paquet M, Witcher M, et al. (2016). Haploinsufficiency of the ESCRT component HD-PTP predisposes to cancer. Cell Rep 15, 1893–1900.
Masyuk AI, Huang BQ, Ward CJ, Gradilone SA, Banales JM, Masyuk TV, Radtke B, Splinter PL, LaRusso NF (2010). Biliary exosomes influence cholangiocyte regulatory mechanisms and proliferation through interaction with primary cilia. Am J Physiol Gastrointest Liver Physiol 299, G990–G999.
Mathieu M, Martin-Jaular L, Lavieu G, Thery C (2019). Specificities of secretion and uptake of exosomes and other extracellular vesicles for cell-to-cell communication. Nat Cell Biol 21, 9–17.
Mattissek C, Teis D (2014). The role of the endosomal sorting complexes required for transport (ESCRT) in tumorigenesis. Mol Membr Biol 31, 111–119.
Mazzone A, Tietz P, Jefferson J, Pagano R, LaRusso NF (2006). Isolation and characterization of lipid microdomains from apical and basolateral plasma membranes of rat hepatocytes. Hepatology 43, 287–296.
Mierzwa B, Gerlich DW (2014). Cytokinetic abscission: molecular mechanisms and temporal control. Dev Cell 31, 525–538.
Mierzwa BE, Chiaruttini N, Redondo-Morata L, von Filseck JM, Konig J, Larios J, Poser I, Muller-Reichert T, Scheuring S, Roux A, Gerlich DW (2017). Dynamic subunit turnover in ESCRT-III assemblies is regulated by Vps4 to mediate membrane remodelling during cytokinesis. Nat Cell Biol 19, 787–798.
O'Hara SP, Tabibian JH, Splinter PL, LaRusso NF (2013). The dynamic biliary epithelia: molecules, pathways, and disease. J Hepatol 58, 575–582.
Olaizola P, Lee-Law PY, Arbelaiz A, Lapitz A, Perugorria MJ, Bujanda L, Banales JM (2018). MicroRNAs and extracellular vesicles in cholangiopathies. Biochim Biophys Acta 1864, 1293–1307.

Parkinson MD, Piper SC, Bright NA, Evans JL, Boname JM, Bowers K, Lehner PJ, Luzio JP (2015). A non-canonical ESCRT pathway, including histidine domain phosphotyrosine phosphatase (HD-PTP), is used for down-regulation of virally ubiquitinated MHC class I. Biochem J 471, 79–88.

Schneider CA, Rasband WS, Eliceiri KW (2012). NIH Image to ImageJ: 25 years of image analysis. Nat Methods 9, 671–675.

Schoneberg J, Lee IH, Iwasa JH, Hurley JH (2017). Reverse-topology membrane scission by the ESCRT proteins. Nat Rev Mol Cell Biol 18, 5–17.

Shiels A, Bennett TM, Knopf HL, Yamada K, Yoshiura K, Niikawa N, Shim S, Hanson PI (2007). CHMP4B, a novel gene for autosomal dominant cataracts linked to chromosome 20q. Am J Hum Genet 81, 596–606.

Shim JH, Xiao C, Hayden MS, Lee KY, Trombetta ES, Pypaert M, Nara A, Yoshimori T, Wilm B, Erdjument-Bromage H, et al. (2006). CHMP5 is essential for late endosome function and down-regulation of receptor signaling during mouse embryogenesis. J Cell Biol 172, 1045–1056.

Shurtleff MJ, Temoche-Diaz MM, Karfilis KV, Ri S, Schekman R (2016). Y-box protein 1 is required to sort microRNAs into exosomes in cells and in a cell-free reaction. eLife 5, e19276.

Sierra MI, Wright MH, Nash PD (2010). AMSH interacts with ESCRT-0 to regulate the stability and trafficking of CXCR4. J Biol Chem 285, 13990–14004.

Skibinski G, Parkinson NJ, Brown JM, Chakrabarti L, Lloyd SL, Hummerich H, Nielsen JE, Hodges JR, Spillantini MG, Thusgaard T, et al. (2005). Mutations in the endosomal ESCRTIII-complex subunit CHMP2B in frontotemporal dementia. Nat Genet 37, 806–808.

Skotland T, Hessvik NP, Sandvig K, Llorente A (2019). Exosomal lipid composition and the role of ether lipids and phosphoinositides in exosome biology. J Lipid Res 60, 9–18.

Tabibian JH, Trussoni CE, O'Hara SP, Splinter PL, Heimbach JK, LaRusso NF (2014). Characterization of cultured cholangiocytes isolated from livers of patients with primary sclerosing cholangitis. Lab Invest 94, 1126–1133.

Takahashi Y, He H, Tang Z, Hattori T, Liu Y, Young MM, Serfass JM, Chen L, Gebru M, Chen C, et al. (2018). An autophagy assay reveals the ESCRT-III component CHMP2A as a regulator of phagophore closure. Nat Commun 9, 2855.

Tauro BJ, Greening DW, Mathias RA, Mathivanan S, Ji H, Simpson RJ (2013). Two distinct populations of exosomes are released from LIM1863 colon carcinoma cell-derived organoids. Mol Cell Proteomics 12, 587–598.

Thery C, Witwer KW, Aikawa E, Alcaraz MJ, Anderson JD, Andriantsitohaina R, Antoniou A, Arab T, Archer F, Atkin-Smith GK, *et al*. (2018). Minimal information for studies of extracellular vesicles 2018 (MISEV2018): a position statement of the International Society for Extracellular Vesicles and update of the MISEV2014 guidelines. J Extracell Vesicles 7, 1535750.

Trajkovic K, Hsu C, Chiantia S, Rajendran L, Wenzel D, Wieland F, Schwille P, Brugger B, Simons M (2008). Ceramide triggers budding of exosome vesicles into multivesicular endosomes. Science 319, 1244–1247.

Tsuchiya S, Yamabe M, Yamaguchi Y, Kobayashi Y, Konno T, Tada K (1980). Establishment and characterization of a human acute monocytic leukemia cell line (THP-1). Int J Cancer 26, 171–176.

van Niel G, Raposo G, Candalh C, Boussac M, Hershberg R, Cerf-Bensussan N, Heyman M (2001). Intestinal epithelial cells secrete exosome-like vesicles. Gastroenterology 121, 337–349.

Villarroya-Beltri C, Gutierrez-Vazquez C, Sanchez-Cabo F, Perez-Hernandez D, Vazquez J, Martin-Cofreces N, Martinez-Herrera DJ, Pascual-Montano A, Mittelbrunn M, Sanchez-Madrid F (2013). Sumoylated hnRNPA2B1 controls the sorting of miRNAs into exosomes through binding to specific motifs. Nat Commun 4, 2980.

Zhou X, Arthur G (1992). Improved procedures for the determination of lipid phosphorus by malachite green. J Lipid Res 33, 1233–1236.